

COMPETING PHASES AND CRITICAL BEHAVIOR IN THREE COUPLED SPINLESS LUTTINGER LIQUIDS

S.Kundu^{1,2} and V.Tripathi¹

¹*Department of Theoretical Physics, Tata Institute of Fundamental Research, Homi Bhabha Road, Colaba, Mumbai 400005, India and*

²*Département de physique and Institut quantique, Université de Sherbrooke, Sherbrooke, Québec, Canada J1K 2R1*

(Dated: February 23, 2022)

We study electronic phase competition in a system of three coupled spinless Luttinger liquids using abelian bosonization, together with a perturbative renormalization group (RG) analysis. The scaling procedure generates off-diagonal contributions to the phase stiffness matrix, which require both rescaling as well as large rotations of the fields. These rotations, generally non-abelian in nature, are important for correctly obtaining the dominant electronic orders and critical behavior in different parameter regimes. They generate a coupling between different interaction channels even at the tree-level order in the coupling constant scaling equations. We study competing phases in this system, taking into account the aforementioned rotations, and determine its critical behavior in a variety of interaction parameter regimes where perturbative RG is possible. The phase boundaries are found to be of the Berezinskii-Kosterlitz-Thouless (BKT) type, and we specify the parameter regimes where valley-symmetry breaking, chiral orders, and restoration of C_3 symmetry may be observed. We discuss experimental systems where our approach and findings may be relevant.

I. INTRODUCTION

Coupled one-dimensional systems of interacting fermions appear in diverse contexts. They have been used as building blocks for studying higher-dimensional systems, such as cuprate high-temperature superconductors,^{1–6,8–11} due to the availability of controlled nonperturbative methods and numerical techniques for analyzing them. They have also appeared in studies of low-dimensional organic conductors,¹⁴ spin ladders,^{15–22} Mott insulating magnets,²⁴ as well as artificially manufactured structures (such as self-assembled transition metal nanowires²⁵). Systems of three coupled Luttinger liquids have, in general, received comparatively less attention than their two-coupled counterparts, but have been studied in the context of carbon nanotube systems,^{12,13} three-leg spin-tube models,^{31–34,40,41} coupled fermionic chains appearing in spin-ladder materials^{21,27–30} and quasi-1D superconductors such as $K_2Cr_3As_3$.²³ The case of three spinless Luttinger liquids is especially interesting since this is the simplest instance where orders such as chiral superconductivity²⁶ and chiral density wave can arise, which are not possible in the case of Luttinger liquid systems with two or fewer fermionic species. Experimentally, understanding the physics of three coupled spinless Luttinger liquids may be useful in the context of multipocket systems such as bismuth^{43–54}, graphite intercalates^{55,56} and even the newly discovered heavy fermion superconductor UTe_2 ^{68–85} in a strong magnetic field. In the quantum limit, these behave effectively as one-dimensional systems.

Bosonization,^{57,58} together with a scaling treatment, has been a common method for studying the low-energy properties of such systems.^{2,5–10,12,14,35–39} For coupled Luttinger liquid systems with three or more fermionic species, the scaling procedure generically introduces off-diagonal corrections to the stiffness matrix \hat{K} in the quadratic part of the bosonized Hamiltonian (a sine-Gordon model): these corrections have largely been neglected in the existing analyses,^{10,12,23} and need to be taken into account. They carry information about the competition between different interaction channels, which

in turn governs the electronic phase competition and critical behavior in these systems. Although they have been introduced in a study involving two spinful coupled Luttinger liquids,⁵ in the context of competing orders in cuprates, the specific nature of the interactions considered there precludes the existence of chiral orders. On the other hand, the simplest situation where such nontrivial corrections arise, is the case of three coupled spinless Luttinger liquids. In this paper, we perform a one-loop RG analysis for such a system, which takes into account the effects of the off-diagonal corrections by introducing large rotations of the \hat{K} -matrix and small renormalizations of the eigenvalues of \hat{K} . Of these two, the latter affects the scaling dimensions of the interactions, while the former effectively rotates the bosonic fields, which affects the subsequent stages of the scaling. From the solutions of the scaling equations, we identify the most singular susceptibilities, corresponding to different order parameters, which in turn determines the phase diagram. Also, from a numerical scaling analysis of the RG equations, we obtain the critical behavior near the phase transition points.

Our main findings are as follows. We find that the fixed point behavior is dependent both on the relative initial values of the coupling constants and the Luttinger liquid parameter. This is a situation qualitatively different from that of systems with two or less than two fermionic species (where such an interplay between different interaction channels does not appear) and is a direct consequence of the rotations of the stiffness matrices introduced in our approach. Depending upon the relative initial values of the couplings and the Luttinger parameters, we identify the different instabilities in the particle-particle and particle-hole channels and the nature of their transitions across phase boundaries. Further, we obtain the conditions under which valley symmetry breaking and intervalley orders may appear in both these channels. The possibility of chiral orders is also discussed in this context.

Our calculations are expected to be relevant for understanding phase transitions and critical phenomena in systems with multiple small Fermi pockets (like graphite intercalates^{55,56}, bismuth^{43–54} and UTe_2 ^{68–85}) subject to quantizing magnetic fields, and cylindrical nanotubes at high fields.¹² In general, such an analysis is applicable

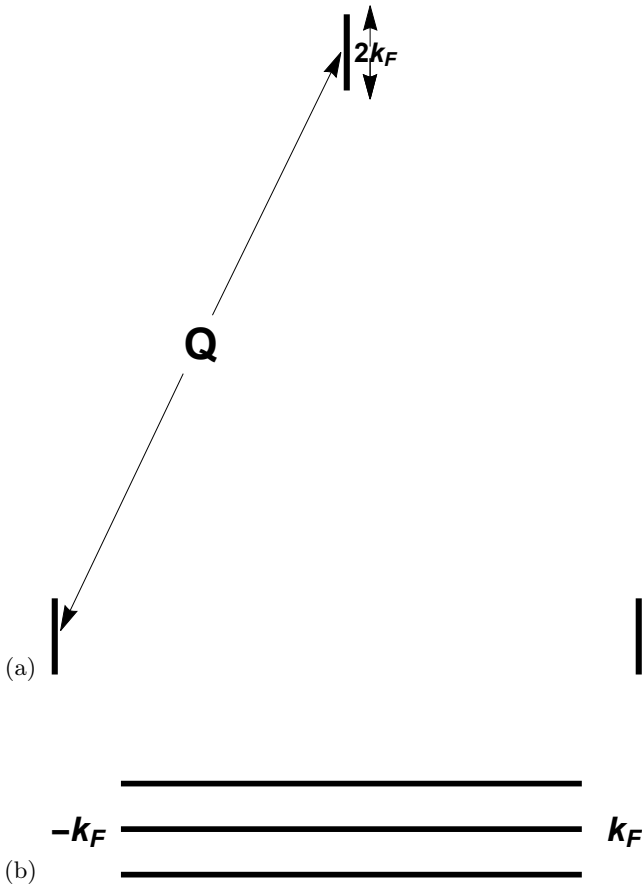


Figure 1. The figure (a) above shows three small Fermi pockets, with Fermi momentum k_F , separated by a vector Q in momentum space such that $Q \gg k_F$, which is illustrative of the situation being considered in the present analysis. In contrast to this, in (b), each Fermi point comprises three flavors of fermions.

for studies of competing phases in three coupled one-dimensional systems where the instability occurs at energy scales much smaller than the chemical potential. However, in situations where the instabilities appear at higher energy scales, other approaches such as the parquet renormalization group approach^{59–61} are more suitable.

The rest of the paper is organized as follows. Sec-II introduces the fermionic Hamiltonian with most generic interactions, describes the bosonization procedure and presents the bosonized Hamiltonian. Sec-III describes the renormalization group procedure used in our analysis, which takes into account both the renormalizations of the eigenvalues of \hat{K} as well as the large rotations of the \hat{K} -matrices. In Sec-IV, we introduce test vertices corresponding to different order parameter fields and study their evolution under the renormalization group, to determine the possible instabilities in different channels. Finally, Sec-V presents a discussion of our results, conclusions and future directions.

II. INTERACTING MODEL AND BOSONIZATION

The fermionic Hamiltonian consists of two parts,

$$H = H_0 + H_{int}$$

where the noninteracting part is the three-band tight-binding model describing electron hopping while the interacting part originates from electron-electron interactions. The non-interacting Hamiltonian in momentum space is given by

$$H_0 = \sum_{km} \epsilon_{km} c_{km}^\dagger c_{km}$$

where the band index $m = 0, \pm 1$, and c_{km} (c_{km}^\dagger) is the electron annihilation (creation) operator for the band m . Near the Fermi points, the energy dispersion can be linearized as $\epsilon_{km} = v_{Fm}(k - k_{Fm})$ where v_{Fm} is the Fermi velocity and k_{Fm} is the Fermi momentum. We assume the Fermi momenta k_{Fm} for the three bands to be identical. We consider generic density-density type of interactions, and expand the three spinless fermionic fields in the vicinity of the two Fermi points. We are interested in situations that physically correspond to partially filled bands, so that Umklapp scattering between the two Fermi points for a given band is not relevant. However, since we would like our model to be relevant for systems with multiple nested Fermi pockets with a nesting vector equal to half a reciprocal lattice vector (such as in the case of bismuth), we do allow the possibility of two-particle Umklapp scattering between pockets, such that the total momentum transferred corresponds to a reciprocal lattice vector. This situation is illustrated in figure 1(a) (In contrast, in figure 1(b), each Fermi point corresponds to three flavors of fermions).

With these assumptions, the interaction part of the Hamiltonian has the following form,

$$\begin{aligned}
H_{int} = & \sum_{p,m} (g_1^{(1)} \psi_{pm}^\dagger \psi_{\bar{p}\bar{m}}^\dagger \psi_{pm} \psi_{\bar{p}\bar{m}} + g_1^{(2)} \psi_{pm}^\dagger \psi_{\bar{p}\bar{m}}^\dagger \psi_{\bar{p}\bar{m}} \psi_{pm} \\
& + g_1^{(3)} \psi_{pm}^\dagger \psi_{\bar{p}\bar{m}}^\dagger \psi_{\bar{p}\bar{m}} \psi_{\bar{p}\bar{m}} + g_1^{(4)} \psi_{pm}^\dagger \psi_{\bar{p}\bar{m}}^\dagger \psi_{pm} \psi_{\bar{p}\bar{m}} \\
& + g_2^{(1)} \psi_{pm}^\dagger \psi_{\bar{p}\bar{m}}^\dagger \psi_{\bar{p}\bar{m}} \psi_{\bar{p}\bar{m}} + g_2^{(2)} \psi_{pm}^\dagger \psi_{\bar{p}\bar{m}}^\dagger \psi_{\bar{p}\bar{m}} \psi_{pm} \\
& + g_2^{(3)} \psi_{pm}^\dagger \psi_{\bar{p}\bar{m}}^\dagger \psi_{\bar{p}\bar{m}} \psi_{\bar{p}\bar{m}} + g_2^{(4)} \psi_{pm}^\dagger \psi_{\bar{p}\bar{m}}^\dagger \psi_{\bar{p}\bar{m}} \psi_{pm} \\
& + g_3^{(1)} \psi_{pm}^\dagger \psi_{\bar{p}\bar{m}}^\dagger \psi_{\bar{p}\bar{m}} \psi_{\bar{p}\bar{m}} + g_3^{(2)} \psi_{pm}^\dagger \psi_{\bar{p}\bar{m}}^\dagger \psi_{\bar{p}\bar{m}} \psi_{\bar{p}\bar{m}} \\
& + g_3^{(3)} \psi_{pm}^\dagger \psi_{\bar{p}\bar{m}}^\dagger \psi_{\bar{p}\bar{m}} \psi_{\bar{p}\bar{m}} + g_3^{(4)} \psi_{pm}^\dagger \psi_{\bar{p}\bar{m}}^\dagger \psi_{\bar{p}\bar{m}} \psi_{\bar{p}\bar{m}} \\
& + g_4^{(1)} \psi_{pm}^\dagger \psi_{\bar{p}\bar{m}}^\dagger \psi_{pm} \psi_{\bar{p}\bar{m}} + g_4^{(2)} \psi_{pm}^\dagger \psi_{\bar{p}\bar{m}}^\dagger \psi_{\bar{p}\bar{m}} \psi_{pm} \\
& + g_4^{(3)} \psi_{pm}^\dagger \psi_{\bar{p}\bar{m}}^\dagger \psi_{pm} \psi_{pm} + g_4^{(4)} \psi_{pm}^\dagger \psi_{\bar{p}\bar{m}}^\dagger \psi_{\bar{p}\bar{m}} \psi_{pm}), \tag{1}
\end{aligned}$$

where $p = 1(-1)$ refers to right (left) moving fermions, and $m = 0, 1, -1$ denotes the bands and $\bar{m} \neq m$. The three bands are regarded as identical, for simplicity. The above model is C_3 symmetric under the permutation of the three bands. To study the low-energy behavior, we shall utilize the standard bosonization technique to analyze the continuum fermion model. We now bosonize the fermionic model using the abelian bosonization prescription,

$$\psi_{pm} = \frac{\eta_{pm}}{\sqrt{2\pi a}} \exp[ipk_{Fm}x] \exp[-ip\sqrt{\pi}\varphi_{pm}], \tag{2}$$

where k_{Fm} is the Fermi momentum for band m , a is a cutoff of the order of the lattice constant, and $p = 1(-1)$ stands for the $R(L)$ branch. The Majorana Klein factors $\eta_{R/Lm}$ satisfy

$$\{\eta_{Rm}, \eta_{Rm'}\} = 2\delta_{mm'}$$

$$\{\eta_{Lm}, \eta_{Lm'}\} = 2\delta_{mm'}$$

$$\{\eta_{Rm}, \eta_{Lm'}\} = 0.$$

We adopt the following convention for the Klein factors, following Ref. 23,

$$\eta_{mp}\eta_{\bar{m}p} = \eta_{0p}\eta_{mp} = im_p,$$

$$\eta_{mp}\eta_{m\bar{p}} = \eta_{0p}\eta_{0\bar{p}} = ip,$$

$$\eta_{mp}\eta_{\bar{m}\bar{p}} = \eta_{0p}\eta_{m\bar{p}} = im,$$

where $p, m = \pm 1$. The chiral fields φ_{pm} can be written in terms of nonchiral fields ϕ_m and θ_m as $\varphi_{pm} = \phi_m - p\theta_m$, and their gradients are proportional to the fermionic density and current operators, respectively, i.e.,

$$\begin{aligned} \nabla\phi_m &\propto \psi_{Rm}^\dagger\psi_{Rm} + \psi_{Lm}^\dagger\psi_{Lm} \\ \nabla\theta_m &\propto \psi_{Rm}^\dagger\psi_{Rm} - \psi_{Lm}^\dagger\psi_{Lm}. \end{aligned} \quad (3)$$

We collect all quadratic bosonic terms together, which we henceforth call the “noninteracting” part. The rest consist of sine-Gordon terms (see below) that we denote as interactions.

We diagonalize the quadratic part of the bosonic Hamiltonian by transforming to new bosonic fields $\tilde{\phi}_i$ given by²³

$$\begin{pmatrix} \phi_1 \\ \phi_{-1} \\ \phi_0 \end{pmatrix} = \begin{pmatrix} \frac{1}{\sqrt{2}} & \frac{1}{\sqrt{6}} & \frac{1}{\sqrt{3}} \\ -\frac{1}{\sqrt{2}} & \frac{1}{\sqrt{6}} & \frac{1}{\sqrt{3}} \\ 0 & -\frac{2}{\sqrt{6}} & \frac{1}{\sqrt{3}} \end{pmatrix} \begin{pmatrix} \tilde{\phi}_1 \\ \tilde{\phi}_{-1} \\ \tilde{\phi}_0 \end{pmatrix},$$

and likewise for the fields θ_i . The “noninteracting” part of the Hamiltonian can then be written as

$$H_0^B = \frac{1}{2} \int dx \sum_{\mu} v_{\mu} (K_{\mu} (\nabla\tilde{\phi}_{\mu})^2 + \frac{1}{K_{\mu}} (\nabla\tilde{\theta}_{\mu})^2), \quad (4)$$

where $\mu = 0, 1, -1$. Note our convention for K_{μ} differs from the one commonly used in the literature, where K_{μ}^{-1} takes the place of K_{μ} . We have, for the bare couplings,

$$\begin{aligned} v_{\pm 1} K_{\pm 1} &= v_F - \frac{1}{2\pi} (G_2 - G_1) \equiv v_{\perp} K_{\perp} \\ v_0 K_0 &= v_F - \frac{1}{2\pi} (G_2^0 - G_1^0) \\ v_{\perp} &= \sqrt{(v_F - \frac{1}{2\pi} (G_2 - G_1))(v_F + \frac{1}{2\pi} (G_1 + G_2))} \\ K_{\perp} &= \sqrt{\frac{1 - \frac{1}{2\pi v_F} (G_2 - G_1)}{1 + \frac{1}{2\pi v_F} (G_1 + G_2)}} \\ v_0 &= \sqrt{(v_F - \frac{1}{2\pi} (G_2^0 - G_1^0))(v_F + \frac{1}{2\pi} (G_1^0 + G_2^0))} \\ K_0 &= \sqrt{\frac{1 - \frac{1}{2\pi v_F} (G_2^0 - G_1^0)}{1 + \frac{1}{2\pi v_F} (G_1^0 + G_2^0)}} \end{aligned}$$

where $G_1 = g_1^{(4)} - g_2^{(4)} + g_4^{(4)}$, $G_2 = -g_1^{(1)} + g_2^{(2)} + g_4^{(1)} - g_4^{(2)}$, $G_1^0 = -2g_1^{(4)} + 2g_2^{(4)} + g_4^{(4)}$ and $G_2^0 = 2g_1^{(1)} - 2g_2^{(2)} + g_4^{(1)} - g_4^{(2)}$. The twofold degeneracy of the eigenvalues of the stiffness matrix \hat{K} is a consequence of the C_3 rotational symmetry of the quadratic part of the Hamiltonian. Following the strategy of Ref. 6, we study the scaling of

the quantities $K_{0,\pm}^{\phi} = v_{0,\pm} K_{0,\pm}$ and $K_{0,\pm}^{\theta} = \frac{v_{0,\pm}}{K_{0,\pm}}$, assuming an initial condition $v_{0,\pm 1} = 1$. We now define new rescaled fields $\tilde{\psi}_{0,\pm 1} = \sqrt{K_{0,\pm}^{\phi}} \tilde{\phi}_{0,\pm 1}$ and $\tilde{\vartheta}_{0,\pm 1} = \sqrt{K_{0,\pm}^{\theta}} \tilde{\theta}_{0,\pm 1}$. Such a rescaling makes the stiffness matrix \hat{K} proportional to the identity matrix. During the RG process, we will find that small diagonal and off-diagonal corrections are introduced to the stiffness matrix, and it has a real symmetric form, that we denote by $Z_{\mu\nu}$.

After bosonization, the “interacting” part of the bosonized Hamiltonian has the form of coupled sine-Gordon terms

$$H_{int}^B = \sum_{\alpha} g_{\alpha} \cos(a_i^{(\alpha)} \tilde{\psi}_i) + \sum_{\beta} g_{\beta} \cos(A_i^{(\beta)} \tilde{\vartheta}_i), \quad (5)$$

where $\alpha = 1 - 3, 7 - 9$ and $\beta = 4 - 6$, and the coefficients,

$$a^{(1)} = \left(\frac{2\sqrt{2}\sqrt{\pi}}{\sqrt{K_{\perp}^{\phi}}}, 0, 0 \right),$$

$$a^{(2)} = \left(\frac{\sqrt{2}\sqrt{\pi}}{\sqrt{K_{\perp}^{\phi}}}, \frac{\sqrt{6}\sqrt{\pi}}{\sqrt{K_{\perp}^{\phi}}}, 0 \right),$$

$$a^{(3)} = \left(\frac{\sqrt{2}\sqrt{\pi}}{\sqrt{K_{\perp}^{\phi}}}, -\frac{\sqrt{6}\sqrt{\pi}}{\sqrt{K_{\perp}^{\phi}}}, 0 \right),$$

$$a^{(7)} = \left(0, \frac{4\sqrt{\pi}}{\sqrt{6}\sqrt{K_{\perp}^{\phi}}}, \frac{4\sqrt{\pi}}{\sqrt{3}\sqrt{K_0^{\phi}}} \right),$$

$$a^{(8)} = \left(\frac{\sqrt{2}\sqrt{\pi}}{\sqrt{K_{\perp}^{\phi}}}, \frac{2\sqrt{\pi}}{\sqrt{6}\sqrt{K_{\perp}^{\phi}}}, -\frac{4\sqrt{\pi}}{\sqrt{3}\sqrt{K_0^{\phi}}} \right),$$

$$a^{(9)} = \left(\frac{\sqrt{2}\sqrt{\pi}}{\sqrt{K_{\perp}^{\phi}}}, -\frac{2\sqrt{\pi}}{\sqrt{6}\sqrt{K_{\perp}^{\phi}}}, \frac{4\sqrt{\pi}}{\sqrt{3}\sqrt{K_0^{\phi}}} \right),$$

$$A^{(4)} = \left(\frac{2\sqrt{2}\sqrt{\pi}}{\sqrt{K_{\perp}^{\theta}}}, 0, 0 \right),$$

$$A^{(5)} = \left(\frac{\sqrt{2}\sqrt{\pi}}{\sqrt{K_{\perp}^{\theta}}}, \frac{\sqrt{6}\sqrt{\pi}}{\sqrt{K_{\perp}^{\theta}}}, 0 \right),$$

$$A^{(6)} = \left(\frac{\sqrt{2}\sqrt{\pi}}{\sqrt{K_{\perp}^{\theta}}}, -\frac{\sqrt{6}\sqrt{\pi}}{\sqrt{K_{\perp}^{\theta}}}, 0 \right),$$

where the effective couplings $g_{\alpha}(\alpha = 1 - 9)$ are linear combinations of the couplings $g_i^{(j)}$ (see Appendix A). The validity of the perturbative RG analysis we shall perform below requires the coupling constants g_{α} to be small, and we assume this to be the case for the rest of the paper. However this limitation does not extend to the stiffnesses $K^{\phi,\theta}$, which may depart significantly from the noninteracting value $K^{\phi,\theta} = 1$, remaining within the purview of perturbative RG. Indeed, given our motivation of understanding electronic phase competition in the quantum limit in low-carrier density (and consequently strongly correlated) semimetals such as bismuth, in the rest of the paper we will largely focus on regimes where the stiffnesses appreciably depart from unity. Note that we allow the possibility of the coupling constants in the sine-Gordon model to break the C_3 permutation symmetry in the following analysis. The same can also be done in the quadratic part and the two are equivalent. During the RG procedure, the vectors \hat{a} and \hat{A} , in general, rotate and stretch. The scaling dimensions for the interaction terms in Eq. 5 depend on the values of the Luttinger parameters $K_0^{\phi,\theta}$ and $K_{\perp}^{\phi,\theta}$, and in our analysis, we only retain the most relevant interaction terms (with the smallest scaling dimensions). This further reduces the number of parameters we need to consider in our model.

III. RENORMALIZATION-GROUP ANALYSIS

The renormalization group follows the standard Wilsonian procedure of elimination of fast degrees of freedom, restoration of the cutoff, rescaling of the couplings and the renormalization of the fields. This gives rise to off-diagonal corrections in the stiffness matrices, which then take the form $Z_{\mu\nu}$. To keep the Gaussian fixed point unchanged, we rotate the $Z_{\mu\nu}^{\theta,\phi}$ matrices, to diagonalize them, and then rescale the fields $\tilde{\phi}_i$ or $\tilde{\theta}_i$ (using the eigenvalues of these matrices) such that the matrices become proportional to identity. Note that the above rotation does not change the scaling dimensions of the sine-Gordon interaction terms. Now, in the new basis obtained after the rotation and the subsequent rescaling of the fields, we once again compute the one-loop corrections and the resulting changes in the diagonal and off-diagonal elements of the stiffness matrices, and repeat the aforementioned steps throughout the RG process. An

$$Z^\phi = \begin{pmatrix} \frac{1}{2} + \sum_\alpha \frac{g_\alpha^2 dy}{16\pi} ((a_1^{(\alpha)})^2 + (a_{-1}^{(\alpha)})^2)(a_1^{(\alpha)})^2 & \sum_\alpha \frac{g_\alpha^2 dy}{16\pi} ((a_1^{(\alpha)})^2 + (a_{-1}^{(\alpha)})^2)(a_1^{(\alpha)})(a_{-1}^{(\alpha)}) & 0 \\ \sum_\alpha \frac{g_\alpha^2 dy}{16\pi} ((a_1^{(\alpha)})^2 + (a_{-1}^{(\alpha)})^2)(a_1^{(\alpha)})(a_{-1}^{(\alpha)}) & \frac{1}{2} + \sum_\alpha \frac{g_\alpha^2 dy}{16\pi} ((a_1^{(\alpha)})^2 + (a_{-1}^{(\alpha)})^2)(a_{-1}^{(\alpha)})^2 & 0 \\ 0 & 0 & \frac{1}{2} \end{pmatrix}. \quad (6)$$

Note that the above matrix is block-diagonal - a consequence of the nature of the interaction terms and/or approximations employed in the parameter regimes considered in our analysis. While the corrections accumulated are infinitesimal, the rotations involved in restoring the matrices with off-diagonal contributions are finite rotations which cannot be accounted for in the RG flow equations. In our approach, we are always in the rotating frame, where these large rotations are absent, and only small incremental changes to the components along the field directions need to be tracked. These amount to slow changes in the orientation and length, in the rotating frame, upon scaling. In the limit where $K_0^\phi \ll K_\perp^\phi$, we find that we only need to retain the couplings g_α ($\alpha = 1 - 3$), based on their lower scaling dimensions. In this case, we calculate one-loop corrections to the Z^ϕ matrices due to the terms g_1 , g_2 and g_3 in the interaction Hamiltonian, and likewise, to the Z^θ matrices due to the terms g_4 , g_5 and g_6 . The corresponding matrix turns out to be block-diagonal due to the symmetry of the interaction terms in this regime. On the other hand, in the limit where $K_\perp^\phi \ll K_0^\phi$, only the couplings g_α ($\alpha = 7 - 9$) need to be retained for our analysis. Here we obtain one-loop corrections to the Z^ϕ matrices arising from the couplings g_7 , g_8 and g_9 , and, once again, to the Z^θ matrices due to the terms g_4 , g_5 and g_6 . In this case, the matrix Z^ϕ generally comprises nonzero corrections to every matrix element. However, in the limit $K_\perp^\phi \ll K_0^\phi$, we can drop certain terms and it reduces to a block-diagonal form similar to Eq. 6 above with $\alpha = 7 - 9$.

In our analysis, we track the scaling equations for the interaction couplings, as well as the coefficients of the fields in the sine-Gordon terms. The eigenvalues of the matrix $Z_{\mu\nu}$ in Eq. 6 above are denoted by z_1 , z_{-1} and z_0 . We diagonalize the matrix and then rescale the fields using these eigenvalues. At any given stage of the RG flow, the coefficients of the fields in the cosine terms

equivalent procedure has been followed in Ref. 6, where, instead of keeping the Gaussian fixed point unchanged, the fields are kept unchanged and the renormalization process leads to rotations and stretching of eigenvalues of the $Z_{\mu\nu}^{\theta,\phi}$ matrices. We simplify our analysis by considering the anisotropic limits $K_\perp^\phi \gg K_0^\phi$ or $K_0^\phi \gg K_\perp^\phi$, which allows us to drop certain terms (which have higher scaling dimensions) in the interacting Hamiltonian in Eq. 5 in each of these limits. However, the formulation may be readily extended to the most general case. We note that the anisotropic limits $K_\perp^\phi \gg K_0^\phi$ or $K_0^\phi \gg K_\perp^\phi$ necessarily mean we are far from the noninteracting limit where $K^{\phi,\theta} \approx 1$. Our remaining analysis thus corresponds to a strong coupling limit of the model. Below we discuss the results obtained by incorporating one-loop corrections to the matrices $Z_{\mu\nu}^\phi$ and $Z_{\mu\nu}^\theta$ in the two aforementioned anisotropic parameter regimes. At any given stage of the RG, the matrix $Z_{\mu\nu}^\phi$, with the one-loop corrections incorporated, is given by

evolve in the manner $a_i^{(\alpha)} \rightarrow \frac{(Ra^{(\alpha)})_i}{\sqrt{z_i}}$, where R is the rotation which diagonalizes the matrix $Z_{\mu\nu}$. We continue to denote the interaction terms as $g_\alpha \cos[\hat{a}_i^{(\alpha)} \tilde{\psi}_i]$ or $g_\alpha \cos[\hat{A}_i^{(\alpha)} \tilde{\vartheta}_i]$, and write down the RG equations for the coefficients $a_i^{(\alpha)}$, $A_i^{(\alpha)}$ and the couplings g_α . As an example, proceeding in incremental steps, the RG equations for the coefficients $a_1^{(1)}$ and $a_{-1}^{(1)}$ (corresponding to the coupling g_1) due to the rescaling process described above, are given by

$$\begin{aligned} \frac{da_1^{(1)}}{dy} &= -a_1^{(1)} \Lambda_1 \\ \frac{da_{-1}^{(1)}}{dy} &= -a_{-1}^{(1)} \Lambda_{-1} \end{aligned} \quad (7)$$

where $z_1 = 1/2 + \Lambda_1 dy$ and $z_{-1} = 1/2 + \Lambda_{-1} dy$, with Λ_1 and Λ_{-1} depending upon all the coupling constants and the coefficients of all the fields in the sine-Gordon terms (see Appendix A, for the explicit expressions of Λ_1 and Λ_{-1}). The leading corrections are quadratic in the coupling constants. This is not surprising since the RG equations of Eq. 7 essentially describe the renormalization of the stiffness constants $K^{\phi,\theta}$, which do not have $O(g)$ tree-level corrections. The RG flow equations for the rest of the components $a_i^{(\alpha)}$ also behave in the same way.

The tree-level contributions to the RG flows for the sine-Gordon couplings g_α are obtained in terms of the scaling dimensions of the respective sine-Gordon terms, and the one-loop contributions are obtained using the Operator Product Expansion (OPE). The RG equations

for the couplings $g_\alpha, \alpha = 1 - 3$ are

$$\begin{aligned} \frac{dg_1}{dy} &= g_1 \left(2 - \frac{1}{4\pi} ((a_1^{(1)})^2 + (a_{-1}^{(1)})^2) \right. \\ &\quad \left. + \frac{1}{8\pi} (a_1^{(2)} a_1^{(3)} + a_{-1}^{(2)} a_{-1}^{(3)}) g_2 g_3 \right), \\ \frac{dg_2}{dy} &= g_2 \left(2 - \frac{1}{4\pi} ((a_1^{(2)})^2 + (a_{-1}^{(2)})^2) \right. \\ &\quad \left. - \frac{1}{8\pi} (a_1^{(1)} a_1^{(3)} + a_{-1}^{(1)} a_{-1}^{(3)}) g_1 g_3 \right), \\ \frac{dg_3}{dy} &= g_3 \left(2 - \frac{1}{4\pi} ((a_1^{(3)})^2 + (a_{-1}^{(3)})^2) \right. \\ &\quad \left. - \frac{1}{8\pi} (a_1^{(1)} a_1^{(2)} + a_{-1}^{(1)} a_{-1}^{(2)}) g_1 g_2 \right) \end{aligned} \quad (8)$$

The RG equations for the rest of the couplings $g_\alpha (\alpha = 4 - 9)$ are also easily obtained and have a similar form as Eq. 8.

One-loop corrections to the RG equations

The $O(g^2)$ one-loop (or OPE) contributions to the renormalization of the coupling constants g_α in Eq. 8 above are perturbatively smaller than the leading tree-level term. In contrast, the OPE contribution is the leading one in the RG equation for the coefficients of the fields in the cosine terms, given in Eq. 7, which determine the scaling dimensions of the interaction terms. In general, one-loop corrections can have a significant effect on the RG flows when the tree-level term is small – the usual motivation for considering higher order corrections in the perturbative RG. However, we found that if the initial values of the sine-Gordon couplings are small, and the initial stiffnesses are appreciably different from unity (reflecting the strongly correlated nature of our problem), the RG equations with or without the one-loop corrections generically give very similar solutions (see Fig. 3). If the initial scaling dimensions of the interaction terms are close to two (i.e. the tree-level contribution is small), or the bare values of the couplings are not sufficiently small (so that the one-loop and tree-level terms are comparable), then the one-loop terms need to be taken into account. This requires a separate, more detailed study and is not attempted in the present work.

We solve the coupled differential equations 7 and 8 numerically and obtain the fixed-point values for the various couplings g_α and the coefficients $a_i^{(\alpha)}$. We consider weak repulsive interactions in every channel, and study the nature of the RG flows as a function of the initial conditions on the interactions and the value of the Luttinger liquid parameter $K_\perp^{\phi, \theta}$. In general, we find that the couplings g_α either diverge or flow to zero in the course of the RG flow. From Eq. 7 above, it is clear that the coefficients $a_1^{(\alpha)}$ and $a_{-1}^{(\alpha)}$ obey different RG equations, and show qualitatively different behavior as a function of the RG flow parameter. In other words, the coefficients of the different fields rescale differently in the course of the RG flow, following the rotation of the stiffness matrix.

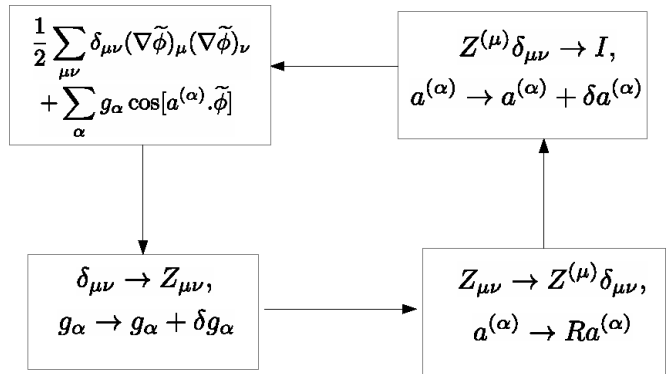


Figure 2. The figure shows a schematic illustration of our renormalization group procedure. The stiffness matrix, which is initially diagonal, develops off-diagonal corrections in the course of the RG flow and takes the general form $Z_{\mu\nu}$. This matrix is diagonalized, which leads to a rotation R of the coefficients $a^{(\alpha)}$ of the sine-Gordon interaction terms. The diagonal elements are then absorbed in the respective sine-Gordon fields, which brings the stiffness matrix back to unity, and leads to a rescaling of the rotated coefficients $a^{(\alpha)}$.

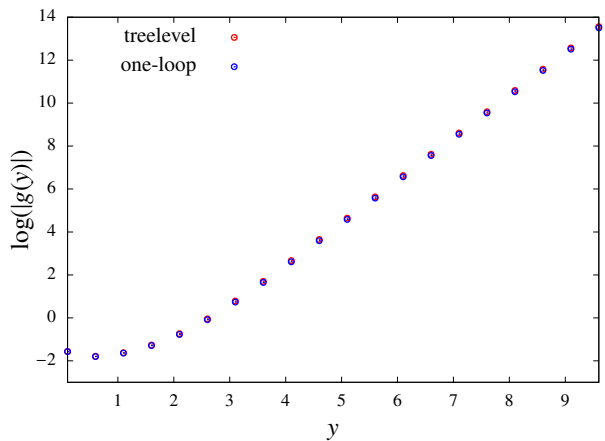


Figure 3. The figure compares the generic scaling behavior of the coupling g_1 with and without considering the effect of the one-loop corrections in the scaling equations for the coupling constants. The parameters have been chosen such that the initial value of the tree-level term exceeds the one-loop contribution. The blue and red circles correspond to the cases with and without the one-loop contributions, respectively. The initial values of the couplings considered are $g_1 = 0.3$, $g_2 = 0.1$, $g_3 = 0.05$, and the value of the Luttinger parameter $K_\perp^\phi = 0.1$. Clearly, the two sets of equations, with or without the one-loop contributions, give very similar results in this regime.

IV. PHASE DIAGRAM AND CRITICAL BEHAVIOR

The order parameters considered in our analysis are fermionic bilinear operators characterized by chirality and band indices. There are two classes of order parameters in our system. These are defined in the particle-hole channel (density wave),²³

$$\text{Re}[O_{ph}^{i0}] \propto \sum_{mm'} \lambda_{mm'}^i \psi_{Rm}^\dagger \psi_{Lm'} + \text{h.c.}, \quad (9)$$

and in the particle-particle channel (superconductivity),

$$\text{Re}[O_{pp}^{i0}] \propto \sum_{mm'} \lambda_{mm'}^i \psi_{Rm}^\dagger \psi_{Lm'}^\dagger + \text{h.c.}, \quad (10)$$

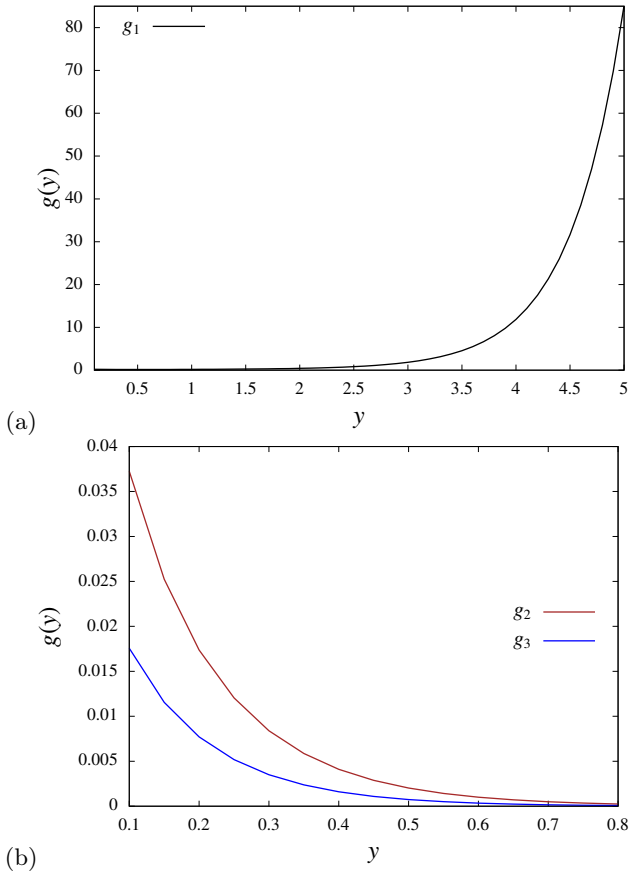


Figure 4. The figure shows the RG flows for the couplings g_1 , g_2 and g_3 for the Luttinger parameter $K_{\perp}^{\phi} = 0.1$ and initial conditions $g_1^0 = 0.3$, $g_2^0 = 0.1$, $g_3^0 = 0.05$. While g_1 grows monotonously (see (a)) under these conditions, g_2 and g_3 show a decline (see (b)). In general, any one or more of the couplings g_{α} may diverge, depending on the initial conditions chosen. The RG flows of the couplings $g_i, i = 4 - 9$ behave in a manner qualitatively similar to that of g_1 , g_2 and g_3 .

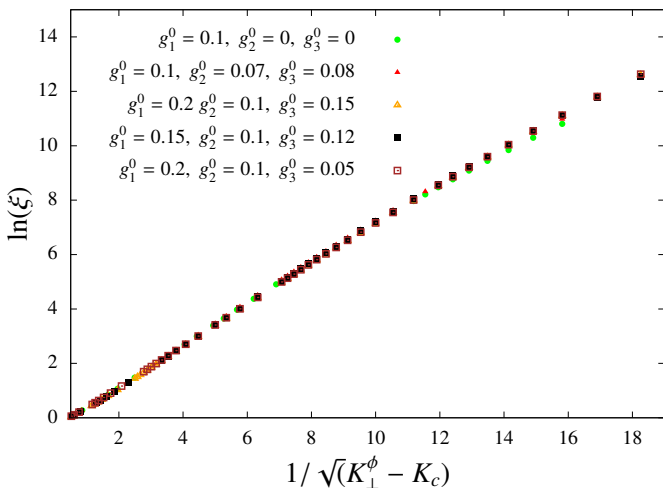


Figure 5. The figure shows a scaling collapse plot of the RG flow parameter $y \sim \ln[\xi]$ (where ξ is the correlation length) as a function of $\frac{1}{\sqrt{K_{\perp}^{\phi} - K_c}}$. K_c denotes the critical value of the

Luttinger liquid parameter K_{\perp}^{ϕ} , where the system undergoes a phase transition. The plot shows results for five different sets of initial conditions on the interactions, with one or more of the couplings g_{α} taking non-zero values initially, and indicates that the phase transitions occurring in this system are continuous in nature and belong to the BKT universality class.

where $\lambda^i (i = 1 \dots 8)$ correspond to the Gell-Mann matrices (see Appendix B for details), λ^0 denotes the 3x3 unit matrix, and $\psi_{pm} (\psi_{pm}^{\dagger})$ is the electron annihilation (creation) operator with chirality p and band m . We follow the convention used by Ref. 23; however, in both the Eqs. 9 and 10, no spin indices are present, due to the spinless nature of the fermions, indicated by the second index being 0 for the order parameters. Note that we consider ordered states arising from scattering or pairing in opposite chiralities in this analysis, and we have checked that equal-chirality interband pairing terms show a qualitatively similar behavior. The order parameters in Eqs. 9 and 10 above are expressed in terms of the bosonic fields. A total of eighteen order parameters are obtained in the particle-hole and particle-particle channels in the spinless case (see Appendix B for expressions of the order parameters in terms of the bosonic fields).

We now discuss the physical meaning of the electronic phases corresponding to the above order parameters. In the anisotropic strong coupling regime that we study (where the initial K_{\perp}^{ϕ} value is often far from unity and the initial g_i are generically unequal), the phases that are obtained are typically associated with the breaking of valley permutation or bond permutation symmetries. However, we also find phases with the C_3 symmetry restored, not slaved to the initial conditions where this is explicitly broken (see Appendix B). Interband pairing in the particle-hole channel corresponds to a bond-ordered (BO) phase, while in the particle-particle channel it gives rise to superconductivity at a finite wavevector (FFLO) equal to the separation between two small Fermi pockets in momentum space, Q . The intraband order parameters correspond to linear combinations of the fermionic bilinears on the three different pockets. One of them is a symmetric linear combination (s -wave, denoted by SW) while the other two are nematic, corresponding to angular momentum $l = 2$ (d -wave order). If we ascribe the angular positions of the three patches in momentum space as $\delta = 0$, $\delta = 2\pi/3$ and $\delta = 4\pi/3$, the phases of the order parameters on the three valleys go either as $\cos(2\delta)$ or $\sin(2\delta)$, both of the d -wave type. It is also possible to have chiral orders, with phases going as $\exp(\pm i\delta)$, as a linear combination of nematic orders. These linear combinations are not unique, and depending on the initial conditions, the actual order parameter may be some combination of these. Intraband pairing in the particle-hole channel has an ordering wavevector $2k_F$, much less than Q , and is generally incommensurate. Depending on the initial conditions, the CDW (charge density wave) order could involve a linear combination of the CDW orders on the three different patches. If C_3 symmetry is not broken, then the orders may have s -wave (uniform CDW, denoted by UCDW), or a doubly degenerate d -wave symmetry (d -density wave). As was the case for superconductivity, the d -density wave order can be either nematic (denoted by NCDW) or chiral type (denoted by cCDW). The order parameters corresponding to different types of order are listed in Table I.

To study the dominant electronic orders, we introduce, in the disordered phase, test vertices corresponding to various order parameter fluctuations and determine how they grow or shrink upon scaling. The evolution of any particular order parameter is governed by a certain combination of couplings, and the one with the smallest scaling dimension, such that the divergence is strongest upon scaling, is the dominant order. Those order parameters

that initially have a large scaling dimension do not grow under scaling and correspond to short-range order. We also take into account the corrections to the scaling dimensions to leading order, $O(g)$ in the couplings, as these terms sometimes lead to shifts in the scaling dimensions of order parameters that have identical RG equations at the tree-level order, resulting in the lifting of degeneracies, with one of them becoming long-range ordered and the other short-range ordered (see Appendix B).

In order to determine the winning order parameters, we consider the behavior of the couplings g_α and the corresponding coefficients of the fields $a_i^{(\alpha)}$ near the fixed point of the RG for a given set of initial conditions and find that both quantities play a crucial role in deciding the nature of the dominant electronic orders. In some cases, we find that none of the order parameters we studied grows under RG, implying the absence of any quasi-long range ordered state despite the presence of interactions. Such situations also come up in the context of floating phases in coupled sine-Gordon models. The advantage of our method is that it not only gives us the dominant order parameters, but also yields the scaling dimension at the fixed point which is essentially the exponent of power law correlations of the order parameter fields in the quasi-long range ordered state. Later, we will show that the transitions, where they occur, belong to the Berezinskii-Kosterlitz-Thouless (BKT) universality class, and that the correlation functions diverge upon approaching the critical point, in accordance with the BKT law.

We classify the nature of the dominant orders in different parameter regimes depending upon the relative sizes of K_\perp^ϕ and K_0^ϕ , considering the two broad classes of parameters, $K_0^\phi \gg K_\perp^\phi$ and $K_\perp^\phi \gg K_0^\phi$. Clearly, this implies some K_\perp^ϕ values must necessarily take values far from the noninteracting point $K_\perp^\phi = 1$, i.e., we are in a strong-correlation regime that is nevertheless accessible by perturbative RG. Within each of these classes, we further examine situations with either $K_0^\phi \gg 1$ or $K_0^\phi \ll 1$. The case with $K_0^\phi \sim 1$, involving a competition between different types of orders, depending upon the initial conditions, requires a more detailed study, and has not been addressed here. In the regime where $K_0^\phi \gg K_\perp^\phi$ and $K_0^\phi \ll 1$, the dominant instabilities are found in the intraband particle-particle channel. Similarly, in the regime where $K_\perp^\phi \gg K_0^\phi$ and $K_0^\phi \gg 1$, the dominant instabilities are found in the intraband particle-hole channel. Note that in these two parameter regimes, K_\perp^ϕ is automatically constrained to be numerically very small or very large. We now consider the remaining two cases, which allow us to tune K_\perp^ϕ over a wide range of values, giving rise to both intraband and interband orders.

We find that for $K_0^\phi \gg K_\perp^\phi$ and $K_0^\phi \gg 1$, the particle-hole orders are more relevant than the particle-particle orders, due to smaller scaling dimensions of the corresponding order parameters, and for $K_\perp^\phi \gg K_0^\phi$ and $K_0^\phi \ll 1$, the particle-particle orders are likewise found to be more important. Within the regimes considered by us, the phase diagram is affected primarily by two factors: the magnitude of the Luttinger liquid parameter K_\perp^ϕ and the set of initial conditions considered for the interactions g_α . The nature of the phase transitions is studied using a numerical scaling analysis. The scaling of the correlation length ξ at the critical point is determined by identifying the characteristic scale y where the couplings

$g_\alpha(y)$ cross a designated value ≥ 1 . We obtain continuous transitions as a function of K_\perp^ϕ , belonging to the Berezinskii-Kosterlitz-Thouless (BKT) universality class, which is confirmed by demonstrating the universal BKT scaling collapse for the behavior of the correlation length close to the critical point (see Fig. 5). Note that the critical value K_c of the Luttinger parameter K_\perp^ϕ is different for different initial conditions on the couplings g_α , as shown in Fig. 5, each of which give rise to the same critical behavior.

Below we discuss the salient features of the phase diagram for the aforementioned two parameter regimes, $K_0^\phi \gg K_\perp^\phi$ and $K_0^\phi \gg 1$, or $K_0^\phi \ll K_\perp^\phi$ and $K_0^\phi \ll 1$, each corresponding to a range of values of K_\perp^ϕ . Since K_\perp^θ is inversely related to K_\perp^ϕ in our model, it does not constitute an independent parameter in the phase diagram.

$K_\perp^\phi \ll 1$: In this regime, for $K_0^\phi \ll K_\perp^\phi$ and $K_0^\phi \ll 1$, the intraband particle-particle orders (SW, Nematic, Chiral) are found to be more relevant, whereas for $K_0^\phi \gg K_\perp^\phi$ and $K_0^\phi \gg 1$, no electronic orders are present when we consider extremely small values of K_\perp^ϕ , and for larger values of K_\perp^ϕ , a particular pair of interband particle-hole orders (BO) dominates, depending upon the initial conditions being considered for the interactions.

$K_\perp^\phi \sim 1$: For $K_\perp^\phi \sim 1$, various intraband and interband particle-particle (FFLO, SW, Nematic, Chiral) orders compete with each other in the regime $K_0^\phi \ll K_\perp^\phi$ and $K_0^\phi \ll 1$, and likewise, various particle-hole (UCDW, NCDW, cCDW, BO) orders compete with each other in the regime $K_0^\phi \gg K_\perp^\phi$ and $K_0^\phi \gg 1$, and it is in this part of the phase diagram that the winning phases are dependent most sensitively on the initial conditions chosen for the interactions. However, at $K_\perp^\phi = 1$ for $K_0^\phi \ll K_\perp^\phi$, or very close to this point, the one-loop corrections should be taken into account, and our analysis in this regime requires further work.

$K_\perp^\phi \gg 1$: In this case, for $K_0^\phi \ll K_\perp^\phi$ and $K_0^\phi \ll 1$, a particular pair of interband particle-particle orders (FFLO) is found to dominate, depending on the initial conditions chosen for the interactions, and no order is found to be present when we consider extremely large values of K_\perp^ϕ , whereas for $K_0^\phi \gg K_\perp^\phi$ and $K_0^\phi \gg 1$, the intraband particle-hole orders (UCDW, NCDW, cCDW) are found to be more relevant.

The types of electronic orders occurring in different parameter regimes, considered in our analysis, are schematically shown in Fig. 6.

V. DISCUSSION AND CONCLUSIONS

In summary, we have studied competing electronic phases and phase transitions in a system of three coupled spinless Luttinger liquids using a renormalization group analysis of the bosonized interactions that takes into account off-diagonal contributions arising from one-loop corrections to the stiffness matrices. This is done by introducing a series of rotations and rescalings of the fields (or equivalently, the coefficients of different fields in the sine-Gordon interaction terms) in the course of the RG flow. These rotations and rescalings are found to depend on all the couplings as well as coefficients of all the fields present in the system. They couple the differ-

Type of order		Order parameter	Name of order
Interband	p-p	$O_{pp}^{10}, O_{pp}^{40}, O_{pp}^{60}$	FFLO(wavevector Q)
		$O_{pp}^{20}, O_{pp}^{50}, O_{pp}^{70}$	FFLO(wavevector Q)
	p-h	$O_{ph}^{10}, O_{ph}^{40}, O_{ph}^{60}$	Bond order (BO)(wavevector Q)
		$O_{ph}^{20}, O_{ph}^{50}, O_{ph}^{70}$	Bond order (BO)(wavevector Q)
Intraband	p-p	$O_{pp}^{00}, O_{pp}^{30}, O_{pp}^{80}$	s -wave (SW), Nematic d -wave, Chiral d -wave
	p-h	$O_{ph}^{00}, O_{ph}^{30}, O_{ph}^{80}$	Uniform(U) CDW , nematic (N) d -CDW , chiral (c) d -CDW

Table I. Table showing electronic phases corresponding to each of the order parameters considered in our analysis. Here particle-particle (p-p) refers to superconductivity, while particle-hole (p-h) refers to density wave orders. Interband pairing between different pairs of bands in the particle-hole channel leads to bond order (denoted by BO) while the corresponding pairing in the particle-particle channel leads to a finite-momentum pairing (denoted by FFLO) state with the wavevector Q , equal to the separation between two small Fermi pockets in momentum space. Intraband pairing can correspond to a situation with different phases on different Fermi pockets and lead to uniform charge density wave (denoted by UCDW) or nematic d -density wave order (denoted by NCDW) in the particle-hole channel, and s -wave or nematic d -wave superconductivity in the particle-particle channel. In the case where these different order parameters are degenerate, a combination of them which is chiral in nature gives rise to the lowest energy configuration. In such a situation, a chiral d -density wave (denoted by cCDW) or chiral d -wave superconductivity can be realized. Despite choosing initial conditions that generically break C_3 permutation symmetry, one nevertheless finds that in some parameter regimes (see text, Fig. 6), phases with the C_3 symmetry restored, such as the chiral orders, are dominant.

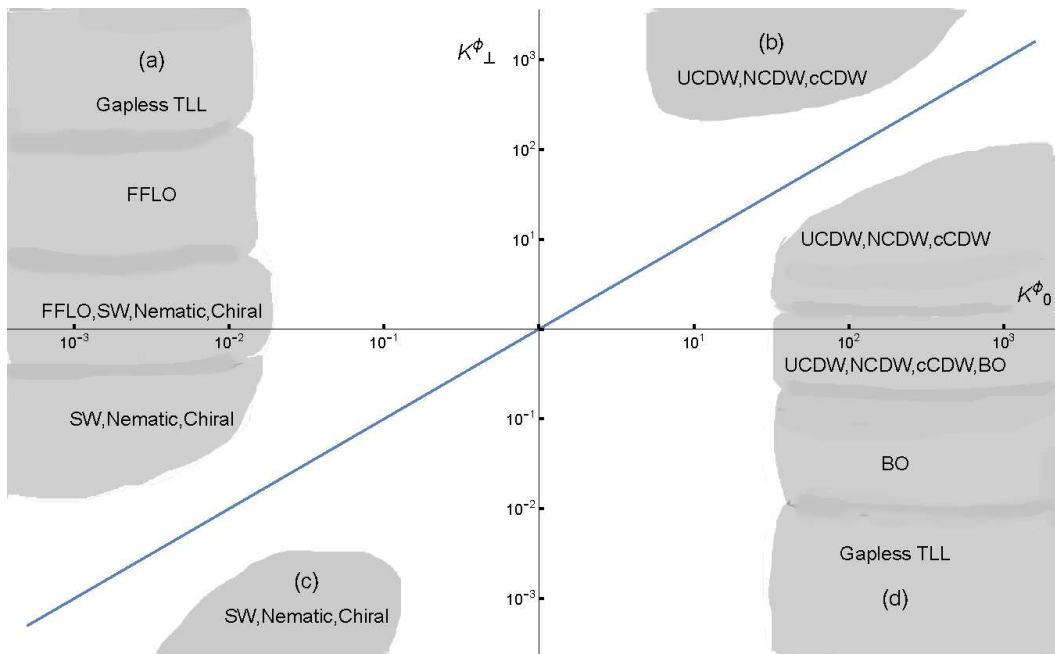


Figure 6. The figure shows the phase diagram for a system of three coupled spinless Luttinger liquids as a function of K_{\perp}^{ϕ} , considering the parameter regimes (a) $K_{\perp}^{\phi} \gg K_0^{\phi}$ and $K_0^{\phi} \ll 1$, where only particle-particle (p-p) orders are considered due to the smaller scaling dimensions of the corresponding order parameters, (b) $K_{\perp}^{\phi} \gg K_0^{\phi}$ and $K_0^{\phi} \gg 1$, where the dominant instabilities belong to the intraband particle-hole channel, (c) $K_0^{\phi} \gg K_{\perp}^{\phi}$ and $K_0^{\phi} \ll 1$ where the dominant instabilities occur in the intraband particle-particle channel, and (d) $K_0^{\phi} \gg K_{\perp}^{\phi}$ and $K_0^{\phi} \gg 1$, where only particle-hole (p-h) orders are considered in our analysis, due to smaller scaling dimensions of the corresponding terms. In cases (a) and (d), we can tune K_{\perp}^{ϕ} over a large range of values, and for $K_{\perp}^{\phi} \sim 1$, various interband and intraband orders compete with one another, the winner being determined by the initial conditions on the interactions. Note that our results are not reliable for $K_{\perp}^{\phi} = 1$ in regime (a), where the one-loop corrections must be taken into account. The orders indicated in the figure have been denoted in the paper as SW for s -wave, FFLO for finite-momentum pairing, UCDW as a CDW order with s -wave symmetry, NCDW as nematic d -density wave, cCDW as chiral d -density wave and BO as bond order. The shaded (gray) portions of the phase diagram demarcate the parameter regimes which can be understood from our analysis. The boundaries of different types of phases are flexible in nature, and can change depending on the initial conditions chosen for the couplings.

ent interaction channels even at the tree-level order. To determine the most dominant electronic orders, we introduce, in the disordered phase, test vertices corresponding to various order parameter fluctuations and study their evolution under the renormalization group. We find that

the overall nature of the winning orders in different parameter regimes is governed by the RG flows of the couplings, as well as those of the coefficients of the fields in the sine-Gordon terms. Notably, for a range of values of the Luttinger liquid parameter K_{\perp}^{ϕ} , which depart appre-

ciably from the noninteracting limit $K_{\perp}^{\phi} = 1$, interband orders involving any one pair of bands are found to be dominant, the specific pair being determined by the initial conditions for the couplings. This is an example of valley symmetry breaking. At $K_{\perp}^{\phi} = 1$ for $K_{\perp}^{\phi} \gg K_0^{\phi}$, one-loop corrections to the RG equations must be taken into account, and this aspect of our analysis requires further work. In the regions where intraband orders are the most relevant, they can be chiral in nature. Such orders restore the original C_3 symmetry of the system, broken explicitly through the initial conditions for the couplings. In the regimes where $K_{\perp}^{\phi} \sim 1$, the nature of the dominant orders is found to be sensitively determined by the initial conditions on the interaction couplings, with multiple orders competing closely. For simplicity of analysis, we have considered the strong correlation regimes of $K_0^{\phi} \gg 1$ or $K_0^{\phi} \ll 1$, and the more involved case of $K_0^{\phi} \sim 1$ has not been discussed, where the particle-particle and particle-hole channels compete with each other and the results are likely to be sensitive to the initial conditions considered. This will be taken up in a future work. We also determine the nature of the phase transitions as a function of the Luttinger parameter K_{\perp}^{ϕ} as well as the initial conditions on the interactions g_{α} using a numerical scaling analysis. The system hosts continuous transitions belonging to the BKT universality class, where the critical value of K_{\perp}^{ϕ} differs with the initial values of the couplings.

From an experimental point of view, our analysis is expected to be relevant for studying electronic interaction effects in semimetals with three small Fermi pockets under conditions of high magnetic fields such that the bands are effectively in the quantum limit, and may be regarded as one-dimensional. Examples include bismuth, the graphite intercalation compounds and possibly the heavy fermion semimetal UTe_2 at high magnetic fields. For bismuth, when the magnetic field is aligned along the highest symmetry axis (the trigonal axis), a field of 9 T allows one to attain the quantum limit putting carriers in their lowest Landau level.⁵³ In this situation, Coulomb interaction effects play an important role in determining the electronic phase. The presence of anomalous features in the magnetization⁶³ and the Nernst response⁴³ of bismuth at high fields, beyond the quantum limit, points towards the importance of examining possible electronic instabilities due to interaction effects in this regime. Furthermore, there has been experimental evidence for valley symmetry breaking at high magnetic fields in bismuth,⁴⁵ and the importance of electron correlations for the same has been recognized. From recent magnetoresistance studies, one or two valleys have been observed to become completely empty above a threshold magnetic field.⁶⁷ Moreover, in semi-metallic bismuth the flow of Dirac fermions along the trigonal axis is extremely sensitive to the orientation of in-plane magnetic field. In the vicinity of the quantum limit, the orientation of magnetic field significantly affects the distribution of carriers in each valley, and the valley polarization is induced by the magnetic field. As the temperature is decreased or the magnetic field increased, the symmetry between the three valleys is spontaneously lost. We expect our technique to be useful for theoretically describing such a situation in bismuth, incorporating the

features known from experiment, and predicting possible electronic instabilities.

In graphite intercalates, the Fermi level often naturally lies in the vicinity of the M-points in the Brillouin zone, which gives rise to another system with three small Fermi pockets. Superconductivity has been predicted and observed experimentally in multiple graphite intercalation compounds, such as CaC_6 , YbC_6 and KC_8 ,⁶⁵ but the possibility of realizing superconductivity or a density wave order under a high magnetic field in such materials has not received much attention in the literature. The case of pure graphite is different; there is evidence for a high field-induced CDW transition⁶⁶ resulting from the enhancement of interactions due to the confinement effect of the magnetic field. However valley-symmetry breaking in graphite occurs between the K and K' points, which is not the subject of this paper. Corresponding field-induced phase transitions in graphite intercalates may, however, be accessible using our analysis.

The recently discovered heavy fermion triplet superconductor UTe_2 ,^{71,72,75-77,82} with a transition temperature $T_{sc}=1.6$ K, exhibits two independent high-field superconducting phases,⁷⁰ one of which has an upper critical field exceeding 65 T, and lies within a field-polarized phase. Such re-entrant superconducting phases are observed for selective ranges of orientation of the field.^{69,70} High-resolution ARPES data for UTe_2 indicates that it has three small Fermi pockets.⁷⁹ A quasi-1D bandstructure has been indicated both by bandstructure calculations and the ARPES studies. Our analysis is expected to be applicable at the highest fields, with electrons fully spin-polarized and in the quantum limit. A field of 65 T corresponds to a magnetic length of about 3.2 nm, which would require a carrier density of about $7 \times 10^{18} \text{ cm}^{-3}$ to be in the quantum limit, typical for semimetallic systems⁴².

In the present work, we have not studied the case where $K_0^{\phi} \sim K_{\perp}^{\phi}$, with the rotations being in general $O(3)$ matrices. The rotation matrices in that case are non-abelian and it would be interesting to see if this gives qualitatively new insights into the problem. In this regime, we also have the possibility of an additional Ising-type symmetry breaking due to the symmetry between the θ and $\tilde{\phi}$ fields when $K_{\perp}^{\phi} = K_0^{\phi} = 1$, which has not been considered in this paper. We hope to study the implications of our approach for the spinful three-band case, and compare our results with Ref. 23, where the rotations of the matrices $Z_{\mu\nu}$ were not taken into account in the RG analysis. We would also like to consider the case of special fillings where intraband Umklapp scattering terms are possible. At first sight, these terms have higher scaling dimensions than the interactions considered by us, and so, at the tree level, they are not relevant. However, more work needs to be done to see the effect they have on the conclusions of this paper.

ACKNOWLEDGMENTS

VT acknowledges DST for a Swarnajayanti grant (No. DST/SJF/PSA-0212012-13).

- ¹ S. Nishimoto, E. Jeckelmann, and D. J. Scalapino, *Phys. Rev. B* **79** (2009).
- ² J. O. Fjaerestad and J. B. Marston, *Phys. Rev. B* **65**, 125106 (2002).
- ³ S. Nishimoto, E. Jeckelmann, and D. J. Scalapino, *Phys. Rev. B* **66**, 245109 (2002).
- ⁴ S. Lee, J. B. Marston, and J. O. Fjaerestad, *Phys. Rev. B* **72**, 075126 (2005).
- ⁵ P. Chudzinski, M. Gabay, and T. Giamarchi, *Phys. Rev. B* **76**, 161101 (2007).
- ⁶ P. Chudzinski, M. Gabay, and T. Giamarchi, *Phys. Rev. B* **78**, 075124 (2008).
- ⁷ R. Assaraf, P. Azaria, M. Caffarel, and P. Lecheminant, *Phys. Rev. B* **60**, 2299 (1999).
- ⁸ M. Tsuchiizu and A. Furusaki, *Phys. Rev. B* **66**, 245106 (2002).
- ⁹ S. Wessel, M. Indergand, A. Lauchli, U. Ledermann, and M. Sgrist, *Phys. Rev. B* **67**, 184517 (2003).
- ¹⁰ C. Wu, W. Vincent Liu, and E. Fradkin, *Phys. Rev. B* **68**, 115104 (2003).
- ¹¹ C. S. O'Hern, T. C. Lubensky, and J. Toner, *Phys. Rev. Lett.* **83**, 2745 (1999).
- ¹² D. Carpentier and E. Orignac, *Phys. Rev. B* **74**, 085409 (2006).
- ¹³ W. DeGottardi, T.-C. Wei, V. Fernandez, and S. Vishveshwara, *Phys. Rev. B* **82**, 155411 (2010).
- ¹⁴ Y. Suzumura and M. Tsuchiizu, *Journal of Physics and Chemistry of Solids* **62**, 93 (2001).
- ¹⁵ S. Chen, H. Buttner, and J. Voit, *Phys. Rev. Lett.* **87**, 087205 (2001).
- ¹⁶ W. Vincent Liu and E. Fradkin, *Phys. Rev. Lett.* **86**, 1865 (2001).
- ¹⁷ D. N. Sheng, O. I. Motrunich, and M. P. A. Fisher, *Phys. Rev. B* **79**, 205112 (2009).
- ¹⁸ M. Sato, *Phys. Rev. B* **76**, 054427 (2007).
- ¹⁹ D. G. Shelton, A. A. Nersesyan, and A. M. Tsvelik, *Phys. Rev. B* **53**, 8521 (1996).
- ²⁰ D. V. Khveshchenko and T. M. Rice, *Phys. Rev. B* **50**, 252 (1994).
- ²¹ D. Cabra, A. Honecker, and P. Pujol, *The European Physical Journal B - Condensed Matter and Complex Systems* **13**, 55 (2000).
- ²² D. Allen, P. Azaria, and P. Lecheminant, *Journal of Physics A: Mathematical and General* **34**, L305 (2001).
- ²³ J.-J. Miao, F.-C. Zhang, and Y. Zhou, *Phys. Rev. B* **94**, 205129 (2016).
- ²⁴ K. Le Hur, A. Soret, and F. Yang, *Phys. Rev. B* **96**, 205109 (2017).
- ²⁵ J.-i. Okamoto and A. J. Millis, *Phys. Rev. B* **85**, 115406 (2012).
- ²⁶ C. Kallin and J. Berlinsky, *Reports on Progress in Physics* **79**, 054502 (2016).
- ²⁷ E. Arrigoni, *Physica Status Solidi (B)* **195**, 425 (1996).
- ²⁸ E. Arrigoni, *Phys. Lett. A* **215**, 91 (1996).
- ²⁹ T. Kimura, K. Kuroki, and H. Aoki, *Phys. Rev. B* **54**, R9608(R) (1996).
- ³⁰ T. Kimura, K. Kuroki, and H. Aoki, *J. Phys. Soc.* **67**, 1377 (1998).
- ³¹ M. Sato, *Phys. Rev. B* **75**, 174407 (2007).
- ³² D. Charrier, S. Capponi, M. Oshikawa, and P. Pujol, *Phys. Rev. B* **82**, 075108 (2010).
- ³³ Y. Zhao, S.-S. Gong, Y.-J. Wang, and G. Su, *Phys. Rev. B* **86**, 224406 (2012).
- ³⁴ Y. Fuji, S. Nishimoto, H. Nakada, and M. Oshikawa, *Phys. Rev. B* **89**, 054425 (2014).
- ³⁵ Y. Tsukamoto, N. Kawakami, Y. Yamashita, and K. Ueda, *Physica B* **281,282**, 540 (2000).
- ³⁶ C. Itoi, S. Qin, and I. Affleck, *Phys. Rev. B* **61**, 6747 (1999).
- ³⁷ P. Azaria, E. Boulat, and P. Lecheminant, *Phys. Rev. B* **61**, 12112 (1999).
- ³⁸ H.C. Lee, P. Azaria, and E. Boulat, *Phys. Rev. B* **69**, 155109 (2004).
- ³⁹ P. Azaria, A.O. Gogolin, P. Lecheminant, and A.A. Nersesyan, *Phys. Rev. Lett.* **83**, 624 (1999).
- ⁴⁰ E. Orignac, R. Citro, and N. Andrei, *Phys. Rev. B* **61**, 11533 (1999).
- ⁴¹ X. Plat, Y. Fuji, S. Capponi, and P. Pujol, *Phys. Rev. B* **91**, 064411 (2015).
- ⁴² K. Akiba, A. Miyake, H. Yaguchi, A. Matsuo, K. Kindo, and M. Tokunaga, *J. Phys. Soc. Jpn.* **84** (2015).
- ⁴³ K. Behnia, L. Balicas, and Y. Kopelevich, *Science* **317**, 1729 (2007).
- ⁴⁴ B. Fauque, B. Vignolle, C. Proust, J.-P. Issi, and K. Behnia, *New Journal of Physics* **11**, 113012 (2009).
- ⁴⁵ R. Kuchler, L. Steinke, R. Daou, M. Brandt, K. Behnia, and F. Steglich, *Nat. Mater.* **13** (2014).
- ⁴⁶ L. Li, J. G. Checkelsky, Y. S. Hor, C. Uher, A. F. Hebard, R. J. Cava, and N. P. Ong, *Science* **321**, 547 (2008).
- ⁴⁷ Y. V. Sharlai and G. P. Mikitik, *Phys. Rev. B* **79**, 081102 (2009).
- ⁴⁸ J. Alicea and L. Balents, *Phys. Rev. B* **79**, 241101 (2009).
- ⁴⁹ B. Fauque, H. Yang, I. Sheikin, L. Balicas, J.-P. Issi, and K. Behnia, *Phys. Rev. B* **79**, 245124 (2009).
- ⁵⁰ M. Matsuo, A. Endo, N. Hatano, H. Nakamura, R. Shirasaki, and K. Sugihara, *Phys. Rev. B* **80**, 075313 (2009).
- ⁵¹ Z. Zhu, B. Fauque, Y. Fuseya, and K. Behnia, *Phys. Rev. B* **84**, 115137 (2011).
- ⁵² B. Seradjeh, J. Wu, and P. Phillips, *Phys. Rev. Lett.* **103**, 136803 (2009).
- ⁵³ H. Yang, B. Fauque, L. Malone, A. B. Antunes, Z. Zhu, C. Uher, and K. Behnia, *Nature Communications* **1**, 47 (2010).
- ⁵⁴ Z. Zhu, B. Fauque, L. Malone, A. B. Antunes, Y. Fuseya, and K. Behnia, *Proceedings of the National Academy of Sciences* **109**, 14813 (2012).
- ⁵⁵ M. Dresselhaus and G. Dresselhaus, *Advances in Physics* **30**, 139 (1981).
- ⁵⁶ F. L. Vogel, "Intercalation compounds of graphite," in *Molecular Metals*, edited by W. E. Hatfield (Springer US, Boston, MA, 1979) pp. 261-279.
- ⁵⁷ S. Rao and D. Sen, arXiv:cond-mat/0005492 (2000).
- ⁵⁸ J. von Delft and H. Schoeller, *Annalen der Physik* **7**, 225 (1998).
- ⁵⁹ N. Furukawa, T. Rice, and M. Salmhofer, *Phys. Rev. Lett.* **81**, 3195 (1998).
- ⁶⁰ C. Honerkamp, M. Salmhofer, N. Furukawa, and T. M. Rice, *Phys. Rev. B* **63**, 035109 (2001).
- ⁶¹ R. Nandkishore, L. Levitov, and A. Chubukov, *Nat. Phys.* **8**, 158 (2012).
- ⁶²
- ⁶³ L. Li, J.G. Checkelsky, Y.S. Hor, C. Uher, A.F. Hebard, R.J. Cava, and N.P. Ong, *Science* **321** (2008).
- ⁶⁴ G.P. Mikitik and Yu. V. Sharlai, *Phys. Rev. B* **91** (2015).
- ⁶⁵ T.E. Weller, M. Ellerby, S.S. Saxena, R.P. Smith, and N.T. Skipper, *Nat. Phys.* **1** (2005).
- ⁶⁶ D. Yoshioka, and H. Fukuyama, *J. Phys. Soc. Jpn* **50** (1981).
- ⁶⁷ Z. Zhu, B. Fauque, K. Behnia, and Y. Fuseya, *J. Phys. Condens. Matter.* **30** (2018).
- ⁶⁸ S. Fujimori, I. Kawasaki, Y. Takeda, H. Yamagami, A. Nakamura, Y. Homma, and D. Aoki, *J. Phys. Soc. Jpn* **88** (2019).
- ⁶⁹ G. Knebel, W. Knafo, A. Pourret, Q. Niu, M. Valiska, D. Braithwaite, G. Lapertot, M. Nardone, A. Zitouni, S. Mishra, I. Sheikin, G. Seyfarth, J.P. Brison, D. Aoki, and J. Flouquet, *J. Phys. Soc. Jpn* **88** (2019).
- ⁷⁰ S. Ran, I-L. Liu, Y.S. Eo, D.J. Campbell, P.M. Neves, W.T. Fuhrman, S.R. Saha, C. Eckberg, H. Kim, D. Graf,

- F. Balakirev, J. Singleton, J. Paglione, and N.P. Butch, Nat. Phys. **15** (2019).
- ⁷¹ S. Ran, C. Eckberg, Q-P. Ding, Y. Furukawa, T. Metz, S.R. Saha, I-L. Liu, M. Zick, H. Kim, J. Paglione, and N.P. Butch, Science **365** (2019).
- ⁷² D. Aoki, A. Nakamura, F. Honda, D. Li, Y. Homma, Y. Shimizu, Y.J. Sato, G. Knebel, J-P. Brison, A. Pourret, D. Braithwaite, G. Lapertot, Q. Niu, bibinfo author M. Valiska, bibinfo author H. Harima, and J. Flouquet, J. Phys. Soc. Jpn **88** (2019).
- ⁷³ A. Miyake, Y. Shimizu, Y.J. Sato, D. Li, A. Nakamura, Y. Homma, F. Honda, J. Flouquet, M. Tokunaga, and D. Aoki, J. Phys. Soc. Jpn **88** (2019).
- ⁷⁴ Y. Tokunaga, H. Sakai, S. Kambe, T. Hattori, N. Higa, G. Nakamine, S. Kitagawa, K. Ishida, A. Nakamura, Y. Shimizu, Y. Homma, D. Li, F. Honda, and D. Aoki, J. Phys. Soc. Jpn **88** (2019).
- ⁷⁵ S. Sundar, S. Gheidi, K. Akintola, A.M. Cote, S.R. Dunsiger, S. Ran, N.P. Butch, S.R. Saha, J. Paglione, and J.E. Sonier, Phys. Rev. B **100** (2019).
- ⁷⁶ T. Metz, S. Bae, S. Ran, I-L. Liu, Y.S. Eo, W.T. Fuhrman, D.S. Agterberg, S.M. Anlage, N.P. Butch, and J. Paglione, Phys. Rev. B **100** (2019).
- ⁷⁷ J. Ishizuka, S. Sumita, A. Daido, and Y. Yanase, Phys. Rev. Lett. **123** (2019).
- ⁷⁸ D. Braithwaite, M. Valiska, G. Knebel, G. Lapertot, J-P. Brison, A. Pourret, M.E. Zhitomirsky, J. Flouquet, F. Honda, and D. Aoki, Communications Physics **2** (2019).
- ⁷⁹ L. Miao, S. Liu, Y. Xu, E. Kotta, C-J. Kang, S. Ran, J. Paglione, G. Kotliar, N.P. Butch, J.D. Denlinger, and A.L. Wray, Phys. Rev. Lett. **124** (2020).
- ⁸⁰ Q. Niu, G. Knebel, D. Braithwaite, D. Aoki, G. Lapertot, G. Seyfarth, J-P. Brison, J. Flouquet, and A. Pourret, arXiv:1907.11118 (2019).
- ⁸¹ V. Hutanu, H. Deng, S. Ran, W.T. Fuhrman, H. Thoma, and N.P. Butch, arXiv:1905.04377 (2019).
- ⁸² L. Jiao, S. Howard, S. Ran, Z. Wang, J.O. Rodriguez, M. Sigrist, Z. Wang, N. Butch, and V. Madhavan, arXiv:1908.02846 (2019).
- ⁸³ S. Ran, H. Kim, I-L. Liu, S. Saha, I. Hayes, T. Metz, Y.S. Eo, J. Paglione, and N.P. Butch, arXiv:1909.06932 (2019).
- ⁸⁴ S. Bae, H. Kim, S. Ran, Y.S. Eo, I-L. Liu, and S. Anlage, arXiv:1909.09032 (2019).
- ⁸⁵ V.G. Yarzhemsky, and E.A. Teplyaskov, arXiv:2001.02963 (2019).

Appendix A: Expressions for bosonic couplings in terms of fermionic couplings

The expressions for the g_α 's in Eq.5 of the main text in terms of the fermionic interactions $g_i^{(j)}$ in Eq.1 are given by-

$$g_1, g_2, g_3 \rightarrow \frac{4}{(2\pi a)^2} (g_2^{(1)} - g_1^{(2)})$$

$$g_4, g_5, g_6 \rightarrow \frac{4}{(2\pi a)^2} (g_3^{(2)} - g_3^{(1)})$$

$$g_7, g_8, g_9 \rightarrow \frac{4}{(2\pi a)^2} (g_1^{(3)} - g_2^{(3)})$$

In the RG equations in Eq. 7 the expressions for Λ_1 and Λ_{-1} are given by

$$\begin{aligned} \Lambda_{\pm 1} = & \frac{1}{32\pi} ((a_1^2 + a_{-1}^2)^2 g_1^2 + (b_1^2 + b_{-1}^2)^2 g_2^2 + (c_1^2 + c_{-1}^2)^2 g_3^2 \pm (a_1^8 g_1^4 + 4a_1^6 a_{-1}^2 g_1^4 + 4a_1^2 a_{-1}^6 g_1^4 + a_{-1}^8 g_1^4 \\ & + (b_1^4 - b_{-1}^4) g_2^4 + 2(b_1^2 + b_{-1}^2)(c_1^2 + c_{-1}^2)(b_{-1}(-c_1 + c_{-1}) + b_1(c_1 + c_{-1}))(b_1(c_1 - c_{-1}) + \\ & b_{-1}(c_1 + c_{-1})) g_2^2 g_3^2 + (c_1^2 + c_{-1}^2)^4 g_3^4 + 8a_1^3 a_{-1} g_1^2 (b_1 b_{-1} (b_1^2 + b_{-1}^2) g_2^2 + c_1 c_{-1} (c_1^2 + c_{-1}^2) g_3^2) + \\ & 8a_1 a_{-1}^3 g_1^2 (b_1 b_{-1} (b_1^2 + b_{-1}^2) g_2^2 + c_1 c_{-1} (c_1^2 + c_{-1}^2) g_3^2) + 2a_1^4 g_1^2 (3a_{-1}^4 g_1^2 + \\ & (b_1^4 - b_{-1}^4) g_2^2 + (c_1^4 - c_{-1}^4) g_3^2) + 2a_{-1}^4 g_1^2 ((-b_1^4 + b_{-1}^4) g_2^2 + (-c_1^4 + c_{-1}^4) g_3^2)^{1/2} \end{aligned}$$

Appendix B: Order parameters, bosonic representation, scaling analysis

In our analysis, the fermionic bilinears for the order parameters are expressed in terms of Gell-Mann matrices, which are a set of eight linearly independent 3×3 traceless Hermitian matrices, given by-

$$\lambda^1 = \begin{pmatrix} 0 & 1 & 0 \\ 1 & 0 & 0 \\ 0 & 0 & 0 \end{pmatrix}, \lambda^2 = \begin{pmatrix} 0 & -i & 0 \\ i & 0 & 0 \\ 0 & 0 & 0 \end{pmatrix}$$

$$\lambda^3 = \begin{pmatrix} 1 & 0 & 0 \\ 0 & -1 & 0 \\ 0 & 0 & 0 \end{pmatrix}, \lambda^4 = \begin{pmatrix} 0 & 0 & 1 \\ 0 & 0 & 0 \\ 1 & 0 & 0 \end{pmatrix}$$

$$\lambda^5 = \begin{pmatrix} 0 & 0 & -i \\ 0 & 0 & 0 \\ i & 0 & 0 \end{pmatrix}, \lambda^6 = \begin{pmatrix} 0 & 0 & 0 \\ 0 & 0 & 1 \\ 0 & 1 & 0 \end{pmatrix}$$

$$\lambda^7 = \begin{pmatrix} 0 & 0 & 0 \\ 0 & 0 & -i \\ 0 & i & 0 \end{pmatrix}, \lambda^8 = \frac{1}{\sqrt{3}} \begin{pmatrix} 1 & 0 & 0 \\ 0 & 1 & 0 \\ 0 & 0 & -2 \end{pmatrix}$$

Below, we list the expressions for the eighteen order parameters in terms of the bosonic fields:

$$\begin{aligned} Re[O_{ph}^{00}] &\propto (2 \cos[\sqrt{2}\sqrt{\pi}\tilde{\phi}_1] \sin[\frac{2\sqrt{\pi}\tilde{\phi}_{-1}}{\sqrt{6}} + \frac{2\sqrt{\pi}\tilde{\phi}_0}{\sqrt{3}} - 2k_F x] + \sin[-\frac{4}{\sqrt{6}}\sqrt{\pi}\tilde{\phi}_{-1} + \frac{2\sqrt{\pi}\tilde{\phi}_0}{\sqrt{3}} - 2k_F x]) \\ Re[O_{ph}^{10}] &\propto \sin[\sqrt{2}\sqrt{\pi}\tilde{\theta}_1] \cos[\frac{2\sqrt{\pi}\tilde{\phi}_{-1}}{\sqrt{6}} + \frac{2\sqrt{\pi}\tilde{\phi}_0}{\sqrt{3}} - 2k_F x] \\ Re[O_{ph}^{20}] &\propto \cos[\sqrt{2}\sqrt{\pi}\tilde{\theta}_1] \cos[\frac{2\sqrt{\pi}\tilde{\phi}_{-1}}{\sqrt{6}} + \frac{2\sqrt{\pi}\tilde{\phi}_0}{\sqrt{3}} - 2k_F x] \\ Re[O_{ph}^{30}] &\propto \sin[\sqrt{2}\sqrt{\pi}\tilde{\phi}_1] \cos[\frac{2\sqrt{\pi}\tilde{\phi}_{-1}}{\sqrt{6}} + \frac{2\sqrt{\pi}\tilde{\phi}_0}{\sqrt{3}} - 2k_F x] \\ Re[O_{ph}^{40}] &\propto \sin[\frac{\sqrt{\pi}\tilde{\theta}_1}{\sqrt{2}} + \frac{3\sqrt{\pi}\tilde{\theta}_{-1}}{\sqrt{6}}] \cos[\frac{\sqrt{\pi}\tilde{\phi}_1}{\sqrt{2}} - \frac{\sqrt{\pi}\tilde{\phi}_{-1}}{\sqrt{6}} + \frac{2\sqrt{\pi}\tilde{\phi}_0}{\sqrt{3}} - 2k_F x] \\ Re[O_{ph}^{50}] &\propto \cos[\frac{\sqrt{\pi}\tilde{\theta}_1}{\sqrt{2}} + \frac{3\sqrt{\pi}\tilde{\theta}_{-1}}{\sqrt{6}}] \cos[\frac{\sqrt{\pi}\tilde{\phi}_1}{\sqrt{2}} - \frac{\sqrt{\pi}\tilde{\phi}_{-1}}{\sqrt{6}} + \frac{2\sqrt{\pi}\tilde{\phi}_0}{\sqrt{3}} - 2k_F x] \\ Re[O_{ph}^{60}] &\propto \sin[\frac{\sqrt{\pi}\tilde{\theta}_1}{\sqrt{2}} - \frac{3\sqrt{\pi}\tilde{\theta}_{-1}}{\sqrt{6}}] \cos[\frac{\sqrt{\pi}\tilde{\phi}_1}{\sqrt{2}} + \frac{\sqrt{\pi}\tilde{\phi}_{-1}}{\sqrt{6}} - \frac{2\sqrt{\pi}\tilde{\phi}_0}{\sqrt{3}} + 2k_F x] \\ Re[O_{ph}^{70}] &\propto \cos[\frac{\sqrt{\pi}\tilde{\theta}_1}{\sqrt{2}} - \frac{3\sqrt{\pi}\tilde{\theta}_{-1}}{\sqrt{6}}] \cos[\frac{\sqrt{\pi}\tilde{\phi}_1}{\sqrt{2}} + \frac{\sqrt{\pi}\tilde{\phi}_{-1}}{\sqrt{6}} - \frac{2\sqrt{\pi}\tilde{\phi}_0}{\sqrt{3}} + 2k_F x] \\ Re[O_{ph}^{80}] &\propto (\cos[\sqrt{2}\sqrt{\pi}\tilde{\phi}_1] \sin[\frac{2\sqrt{\pi}\tilde{\phi}_{-1}}{\sqrt{6}} + \frac{2\sqrt{\pi}\tilde{\phi}_0}{\sqrt{3}} - 2k_F x] - \sin[-\frac{4}{\sqrt{6}}\sqrt{\pi}\tilde{\phi}_{-1} + \frac{2\sqrt{\pi}\tilde{\phi}_0}{\sqrt{3}} - 2k_F x]) \\ Re[O_{pp}^{00}] &\propto (2 \cos[\sqrt{2}\sqrt{\pi}\tilde{\theta}_1] \sin[\frac{2\sqrt{\pi}\tilde{\theta}_{-1}}{\sqrt{6}} + \frac{2\sqrt{\pi}\tilde{\theta}_0}{\sqrt{3}}] - \sin[\frac{4\sqrt{\pi}\tilde{\theta}_{-1}}{\sqrt{6}} - \frac{2\sqrt{\pi}\tilde{\theta}_0}{\sqrt{3}}]) \\ Re[O_{pp}^{10}] &\propto \sin[\sqrt{2}\sqrt{\pi}\tilde{\phi}_1] \cos[\frac{2\sqrt{\pi}\tilde{\theta}_{-1}}{\sqrt{6}} + \frac{2\sqrt{\pi}\tilde{\theta}_0}{\sqrt{3}}] \\ Re[O_{pp}^{20}] &\propto \cos[\sqrt{2}\sqrt{\pi}\tilde{\phi}_1] \cos[\frac{2\sqrt{\pi}\tilde{\theta}_{-1}}{\sqrt{6}} + \frac{2\sqrt{\pi}\tilde{\theta}_0}{\sqrt{3}}] \\ Re[O_{pp}^{30}] &\propto \sin[\sqrt{2}\sqrt{\pi}\tilde{\theta}_1] \cos[\frac{2\sqrt{\pi}\tilde{\theta}_{-1}}{\sqrt{6}} + \frac{2\sqrt{\pi}\tilde{\theta}_0}{\sqrt{3}}] \\ Re[O_{pp}^{40}] &\propto \sin[\frac{\sqrt{\pi}\tilde{\phi}_1}{\sqrt{2}} + \frac{3\sqrt{\pi}\tilde{\phi}_{-1}}{\sqrt{6}}] \cos[\frac{\sqrt{\pi}\tilde{\theta}_1}{\sqrt{2}} - \frac{\sqrt{\pi}\tilde{\theta}_{-1}}{\sqrt{6}} + \frac{2\sqrt{\pi}\tilde{\theta}_0}{\sqrt{3}}] \\ Re[O_{pp}^{50}] &\propto \cos[\frac{\sqrt{\pi}\tilde{\phi}_1}{\sqrt{2}} + \frac{3\sqrt{\pi}\tilde{\phi}_{-1}}{\sqrt{6}}] \cos[\frac{\sqrt{\pi}\tilde{\theta}_1}{\sqrt{2}} - \frac{\sqrt{\pi}\tilde{\theta}_{-1}}{\sqrt{6}} + \frac{2\sqrt{\pi}\tilde{\theta}_0}{\sqrt{3}}] \\ Re[O_{pp}^{60}] &\propto \sin[\frac{\sqrt{\pi}\tilde{\phi}_1}{\sqrt{2}} - \frac{3\sqrt{\pi}\tilde{\phi}_{-1}}{\sqrt{6}}] \cos[\frac{\sqrt{\pi}\tilde{\theta}_1}{\sqrt{2}} + \frac{\sqrt{\pi}\tilde{\theta}_{-1}}{\sqrt{6}} - \frac{2\sqrt{\pi}\tilde{\theta}_0}{\sqrt{3}}] \\ Re[O_{pp}^{70}] &\propto \cos[\frac{\sqrt{\pi}\tilde{\phi}_1}{\sqrt{2}} - \frac{3\sqrt{\pi}\tilde{\phi}_{-1}}{\sqrt{6}}] \cos[\frac{\sqrt{\pi}\tilde{\theta}_1}{\sqrt{2}} + \frac{\sqrt{\pi}\tilde{\theta}_{-1}}{\sqrt{6}} - \frac{2\sqrt{\pi}\tilde{\theta}_0}{\sqrt{3}}] \\ Re[O_{pp}^{80}] &\propto (\cos[\sqrt{2}\sqrt{\pi}\tilde{\theta}_1] \sin[\frac{2\sqrt{\pi}\tilde{\theta}_{-1}}{\sqrt{6}} + \frac{2\sqrt{\pi}\tilde{\theta}_0}{\sqrt{3}}] + \sin[\frac{4\sqrt{\pi}\tilde{\theta}_{-1}}{\sqrt{6}} - \frac{2\sqrt{\pi}\tilde{\theta}_0}{\sqrt{3}}]). \end{aligned} \tag{B1}$$

We further define the order parameters

$$\begin{aligned}
Re[\Delta_{ph}^{10}] &\propto \sin[\sqrt{2}\sqrt{\pi}\widetilde{\phi}_1 + \frac{2\sqrt{\pi}\widetilde{\phi}_{-1}}{\sqrt{6}} + \frac{2\sqrt{\pi}\widetilde{\phi}_0}{\sqrt{3}} - 2k_F x] \\
Re[\Delta_{ph}^{20}] &\propto \sin[\sqrt{2}\sqrt{\pi}\widetilde{\phi}_1 - \frac{2\sqrt{\pi}\widetilde{\phi}_{-1}}{\sqrt{6}} - \frac{2\sqrt{\pi}\widetilde{\phi}_0}{\sqrt{3}} + 2k_F x] \\
Re[\Delta_{ph}^{30}] &\propto \sin[\frac{4\sqrt{\pi}\widetilde{\phi}_{-1}}{\sqrt{6}} - \frac{2\sqrt{\pi}\widetilde{\phi}_0}{\sqrt{3}} + 2k_F x] \\
Re[\Delta_{pp}^{10}] &\propto \sin[\sqrt{2}\sqrt{\pi}\widetilde{\theta}_1 + \frac{2\sqrt{\pi}\widetilde{\theta}_{-1}}{\sqrt{6}} + \frac{2\sqrt{\pi}\widetilde{\theta}_0}{\sqrt{3}}] \\
Re[\Delta_{pp}^{20}] &\propto \sin[\sqrt{2}\sqrt{\pi}\widetilde{\theta}_1 - \frac{2\sqrt{\pi}\widetilde{\theta}_{-1}}{\sqrt{6}} - \frac{2\sqrt{\pi}\widetilde{\theta}_0}{\sqrt{3}}] \\
Re[\Delta_{pp}^{30}] &\propto \sin[\frac{4\sqrt{\pi}\widetilde{\theta}_{-1}}{\sqrt{6}} - \frac{2\sqrt{\pi}\widetilde{\theta}_0}{\sqrt{3}}].
\end{aligned} \tag{B2}$$

corresponding to particle-particle and particle-hole ordering on each of the three individual Fermi pockets, which we track in our RG analysis. The order parameters, introduced as infinitesimal test vertices, scale upon renormalization in the following manner:

$$\begin{aligned}
\frac{dO_{ph}^{10}}{dy} &= (2 - \frac{1}{16\pi}((A_1^{(4)})^2 + (A_{-1}^{(4)})^2 + (a_1^{(7)})^2 + (a_{-1}^{(7)})^2) + \frac{1}{16\pi}g_4((A_1^{(4)})^2 + (A_{-1}^{(4)})^2))O_{ph}^{10}, \\
\frac{dO_{ph}^{20}}{dy} &= (2 - \frac{1}{16\pi}((A_1^{(4)})^2 + (A_{-1}^{(4)})^2 + (a_1^{(7)})^2 + (a_{-1}^{(7)})^2) - \frac{1}{16\pi}g_4((A_1^{(4)})^2 + (A_{-1}^{(4)})^2))O_{ph}^{20}, \\
\frac{dO_{ph}^{40}}{dy} &= (2 - \frac{1}{16\pi}((a_1^{(9)})^2 + (a_{-1}^{(9)})^2 + (A_1^{(5)})^2 + (A_{-1}^{(5)})^2) + \frac{1}{16\pi}g_5((A_1^{(5)})^2 + (A_{-1}^{(5)})^2))O_{ph}^{40}, \\
\frac{dO_{ph}^{50}}{dy} &= (2 - \frac{1}{16\pi}((a_1^{(9)})^2 + (a_{-1}^{(9)})^2 + (A_1^{(5)})^2 + (A_{-1}^{(5)})^2) - \frac{1}{16\pi}g_5((A_1^{(5)})^2 + (A_{-1}^{(5)})^2))O_{ph}^{50}, \\
\frac{dO_{ph}^{60}}{dy} &= (2 - \frac{1}{16\pi}((a_1^{(8)})^2 + (a_{-1}^{(8)})^2 + (A_1^{(6)})^2 + (A_{-1}^{(6)})^2) + \frac{1}{16\pi}g_6((A_1^{(6)})^2 + (A_{-1}^{(6)})^2))O_{ph}^{60}, \\
\frac{dO_{ph}^{70}}{dy} &= (2 - \frac{1}{16\pi}((a_1^{(8)})^2 + (a_{-1}^{(8)})^2 + (A_1^{(6)})^2 + (A_{-1}^{(6)})^2) - \frac{1}{16\pi}g_6((A_1^{(6)})^2 + (A_{-1}^{(6)})^2))O_{ph}^{70}, \\
\frac{d\Delta_{ph}^{10}}{dy} &= (2 - \frac{1}{4\pi}(a_1^2 + a_{-1}^2))\Delta_{ph}^{10}, \\
\frac{d\Delta_{ph}^{20}}{dy} &= (2 - \frac{1}{4\pi}(b_1^2 + b_{-1}^2))\Delta_{ph}^{20}, \\
\frac{d\Delta_{ph}^{30}}{dy} &= (2 - \frac{1}{4\pi}(c_1^2 + c_{-1}^2))\Delta_{ph}^{30}, \\
\frac{dO_{pp}^{10}}{dy} &= (2 - \frac{1}{16\pi}((a_1^{(1)})^2 + (a_{-1}^{(1)})^2 + (A_1^{(7)})^2 + (A_{-1}^{(7)})^2) + \frac{1}{16\pi}g_1((a_1^{(1)})^2 + (a_{-1}^{(1)})^2))O_{pp}^{10}, \\
\frac{dO_{pp}^{20}}{dy} &= (2 - \frac{1}{16\pi}((a_1^{(1)})^2 + (a_{-1}^{(1)})^2 + (A_1^{(7)})^2 + (A_{-1}^{(7)})^2) - \frac{1}{16\pi}g_1((a_1^{(1)})^2 + (a_{-1}^{(1)})^2))O_{pp}^{20}, \\
\frac{dO_{pp}^{40}}{dy} &= (2 - \frac{1}{16\pi}((a_1^{(2)})^2 + (a_{-1}^{(2)})^2 + (A_1^{(9)})^2 + (A_{-1}^{(9)})^2) + \frac{1}{16\pi}g_2((a_1^{(2)})^2 + (a_{-1}^{(2)})^2))O_{pp}^{40}, \\
\frac{dO_{pp}^{50}}{dy} &= (2 - \frac{1}{16\pi}((a_1^{(2)})^2 + (a_{-1}^{(2)})^2 + (A_1^{(9)})^2 + (A_{-1}^{(9)})^2) - \frac{1}{16\pi}g_2((a_1^{(2)})^2 + (a_{-1}^{(2)})^2))O_{pp}^{50}, \\
\frac{dO_{pp}^{60}}{dy} &= (2 - \frac{1}{16\pi}((a_1^{(3)})^2 + (a_{-1}^{(3)})^2 + (A_1^{(8)})^2 + (A_{-1}^{(8)})^2) + \frac{1}{16\pi}g_3((a_1^{(3)})^2 + (a_{-1}^{(3)})^2))O_{pp}^{60}, \\
\frac{dO_{pp}^{70}}{dy} &= (2 - \frac{1}{16\pi}((a_1^{(3)})^2 + (a_{-1}^{(3)})^2 + (A_1^{(8)})^2 + (A_{-1}^{(8)})^2) - \frac{1}{16\pi}g_3((a_1^{(3)})^2 + (a_{-1}^{(3)})^2))O_{pp}^{70}, \\
\frac{d\Delta_{pp}^{10}}{dy} &= (2 - \frac{1}{4\pi}(A_1^2 + A_{-1}^2))\Delta_{pp}^{10}, \\
\frac{d\Delta_{pp}^{20}}{dy} &= (2 - \frac{1}{4\pi}(B_1^2 + B_{-1}^2))\Delta_{pp}^{20}, \\
\frac{d\Delta_{pp}^{30}}{dy} &= (2 - \frac{1}{4\pi}(C_1^2 + C_{-1}^2))\Delta_{pp}^{30},
\end{aligned} \tag{B3}$$

where the coefficients of the fields $\tilde{\phi}_i$ and $\tilde{\theta}_i$ in the sine-Gordon terms representing the different order parameters O_{ph}^{i0}, O_{pp}^{i0} are expressed in terms of $a_i^{(\alpha)}, \alpha = 1 - 3, 7 - 9$ and $A_i^{(\alpha)}, \alpha = 1 - 3, 7 - 9$ respectively. Note that we work in the regimes $K_0^\phi \gg K_\perp^\phi$ or $K_0^\phi \ll K_\perp^\phi$, which enables us to drop terms involving K_0^ϕ compared to those involving K_\perp^ϕ , in different regimes.

Here $a_i^{(\alpha)}, \alpha = 1 - 3, 7 - 9$ and $A_i^{(\alpha)}, \alpha = 4 - 6$ are the usual coefficients of the fields for the interaction couplings g_α as defined in Eq. 5 of the main text. On the other hand, the coefficients $A_i^{(\alpha)}, \alpha = 7 - 9$ are defined in the same way for the fields $\tilde{\theta}_i$ as $a_i^{(\alpha)}, \alpha = 7 - 9$ are defined for the fields $\tilde{\phi}_i$ in Eq. 5. While the latter coefficients for the fields $\tilde{\theta}_i$ do not actually appear in the sine-Gordon terms corresponding to any of the interaction couplings considered by us in Eq. 5, we introduce them here for simplicity, since the coefficients of the fields in some of the order parameters can be expressed neatly in terms of these quantities.

In addition, the coefficients of the fields for the sine-Gordon terms corresponding to the order parameters $\Delta_{pp/ph}^{i0} (i = 1 - 3)$ (see Eq.B2 above) are defined as a_i, b_i, c_i and A_i, B_i, C_i (where $i = 1, -1$), as these cannot be expressed in terms of the coefficients already defined for any of the interaction couplings g_α in Eq. 5. Note that the scaling dimensions for these order parameters do not have any $O(g)$ corrections from any of the nine couplings $g_i, i = 1 - 9$ considered by us. However there are $O(g)$ corrections to their scaling dimensions from other interaction terms with higher scaling dimensions that have been neglected in this analysis. The order parameters $\Delta_{pp/ph}^{i0} (i = 1 - 3)$ simultaneously diverge in certain parameter regimes where K_\perp^ϕ takes extremely large or small values (depending on the type of order being considered) – a manifestation of restoration of the C_3 symmetry that had been explicitly broken through the initial conditions of the RG. The specific nature of order in these enlarged symmetry phases requires consideration of higher order processes that couple the degenerate order parameters, and may have s -wave, d -wave or chiral d -wave symmetry (see main text for discussion).